Hybrid Si_3N_4/VO_2 Modulator Thermally Triggered by a Graphene Microheater

Babak Janjan, Mehdi Miri, Davood Fathi, Mohsen Heidari, and Derek Abbott, *Fellow, IEEE*

***Abstract*—Si_3N_4 has emerged as a prominent material for expanding the capability of silicon photonics to wavelengths below < 1 μm. However, realizing an efficient optical modulator, a key building block for any integrated optics platform, remains a major challenge in Si_3N_4 mainly because this material has a vanishing Pockels coefficient. Here, we propose a compact Si_3N_4 based optical modulator by using a thin VO_2 layer on top of a Si_3N_4 strip waveguide where amplitude modulation is achieved via phase transition of the VO_2 layer. To reduce the actuation time of the temperature-induced VO_2 phase transition, a mono-layer graphene microheater is designed for the active $Si_3N_4VO_2$ waveguide. Our simulations indicate a high extinction ratio of $\sim$8.28 dB/μm with an insertion loss of $\sim$2.8 dB/μm at the design wavelength of 850 nm for the proposed modulator and wideband operation in the wavelength range of 800–900 nm. It is shown that employing the electrical and thermal properties of graphene not only leads to a significant reduction of the power consumption of the device but also, decreases the actuation time compared to previous modulators based on the thermal phase transition of the VO_2.**

***Index Terms*—Graphene, optical modulator, phase-change material, silicon photonics.**

I. Introduction

With a wide bandgap of $\sim$5 eV and wide range transparency down to the wavelength of $\sim$400 nm, and also being fully compatible with CMOS fabrication, silicon nitride (Si_3N_4) is a promising alternative material for the implementation of silicon-photonic systems for applications at wavelengths below 1.1 μm. In this wavelength range, which has many applications in life science and data communication, silicon is highly absorptive [1]. Motivated by these characteristics, many Si_3N_4-based passive functional components such as waveguides, ring resonators, grating couplers [2], [3], arrayed waveguide gratings [4], (de)multiplexers and directional couplers [5] have been demonstrated. Unfortunately, because of its centrosymmetric crystal structure, Si_3N_4 does not exhibit a Pockels coefficient, which is essential for realizing efficient active devices, while the implementation of active devices such as optical modulators is vital in integrated photonic systems. Although the thermo-optic effect of Si_3N_4 is employed to realize active devices, it suffers from inherent drawbacks of low speed, high energy consumption, and large foot-print area [6], [7]. An improved solution is to hybridize the structure with a strong electro-refractive or electro-absorptive layer. In this context, graphene [8], [9], zinc sulfide (ZnS) and zinc oxide (ZnO) [10], and lead zirconate titanate (PZT) [11], [12] have been used. However, optical modulators relying on these materials have large size and need high external voltage and their fabrication is associated with challenges such as Cu diffusion in the underlying CMOS electronics during high-temperature annealing [13].

Another interesting option is to hybridize Si_3N_4 waveguide with phase change materials (PCMs) such as vanadium dioxide (VO_2), which exhibit a reversible phase transition between an insulting and a conducting plane [14]. The insulator-conductor phase transition significantly changes both the real and imaginary parts of the refractive index of VO_2 and can be used to design active devices with improved overall performance. This property of VO_2 material has been employed to realize several active devices such as compact modulators and switches [15]–[27]. The VO_2 phase transition is usually initiated by increasing its temperature above a threshold temperature, applying an electric field stronger than a critical field or by a combination of both effects [22], [24], [25], [28]. In the case of thermal actuation, metal heaters are often used. In these structures, the metal heaters should be placed far from the VO_2 layer to avoid mode disturbance or extra light-absorption induced by the metallic layers that degrade the efficiency of the modulator [16]–[18], [20], [22]. This limits the heat transport efficiency and as a result, these devices suffer the drawback of low-speed modulation speed (and low electrical bandwidth) [16]–[18], [20], [22]. Moreover, a part of the power will be dissipated in an unwanted region that increases the total power consumption of the modulator [22]. Considering the improved performance of VO_2-based active devices in terms of footprint and extinction ratio, the proposal of novel approaches to alleviate the inherent speed limitation of these modulators and increase their modulation speed is of great importance. To overcome this issue, the generated heat should be focused in the VO_2 region, overlap with the optical mode and also transferred and dissipated at high speed. One possible solution is to deposit a very thin metallic layer (in order of few nanometers) on top of the PCM so thin that it does not disturb the optical mode and can increase the temperature of

Manuscript received November 25, 2019; accepted May 19, 2020. Date of publication May 22, 2020; date of current version June 3, 2020. *(Corresponding author: Mehdi Miri.)*

Babak Janjan, Davood Fathi, and Mohsen Heidari are with the School of Electrical and Computer Engineering, Tarbiat Modares University, Tehran 14115-111, Iran (e-mail: b.janjan@modares.ac.ir; d.fathi@modares.ac.ir; mh.heidari@modares.ac.ir).

Mehdi Miri is with the School of Electrical and Computer Engineering, Shiraz University, Shiraz 71348-51154, Iran (e-mail: miri@shirazu.ac.ir).

Derek Abbott is with the School of Electrical and Electronic Engineering, The University of Adelaide, Adelaide, SA 5005, Australia (e-mail: derek.abbott@adelaide.edu.au).

Color versions of one or more of the figures in this article are available online at https://ieeexplore.ieee.org.

Digital Object Identifier 10.1109/JSTQE.2020.2996754

the PCM above the required threshold at high speed [29]. But this places additional constraints on the electrical and optical design of the structure. For example, a very thin metallic layer has high electrical resistance and its temperature rises very fast during the thermal excitation process. Therefore, the waveguide dimensions and the duration of the actuation pulse should be designed in a way to keep the temperature of the metallic layer below its melting point while the temperature of the PCM rises above the threshold value [29]. Application of an ultra-thin two-dimensional material with very high electrical and thermal conductivity and high melting point increases thermal excitation speed and relaxes the above constraint on the waveguide design. Graphene can be considered as a viable choice for this purpose.

Graphene [30]–[33], among the known materials, has the highest thermal conductivity (up to 5300 W/m·K [34]) that suggests excellent heat transfer capability at a very high speed. It has been reported that the use of graphene as the heater can significantly improve the speed [35], [36] and efficiency [35], [37] of the thermo-optic effect of the silicon element due to its extremely high thermal conductivity and direct heat transfer to the underlying material. In this study, we propose a highly efficient and compact hybrid Si_3N_4/VO_2 modulator thermally triggered by a graphene microheater for application at the wavelength of $\lambda = 850$ nm (which is one of the three wavelength windows in optical telecommunications [38]). Our simulations show an extinction ratio of $\sim$8.28 dB/μm for the proposed waveguide. Also, focused heating of the VO_2 through graphene leads to reduced power consumption $\sim$1.5 mW for the VO_2 phase transition that is much lower than that of previous studies [17], [18], [22]. Also, the significant thermal conductivity of graphene reduces the response time of the device to less than 200 ns which is at least one order of magnitude lower than previously reported values for Joule-heating-based VO_2 modulators [22].

The rest of this paper is organized as follows; the structure of the proposed active waveguide and electro-absorption modulator is introduced in the Section 2. The optical design of the active waveguide is provided in the Section 3 and the optical and electrical properties of the modulator are respectively, calculated through 3D-FDTD and electro-thermal simulations. Finally, a summary of the results and conclusions is provided in the Section 4.

II. Proposed Modulator

Fig. 1 depicts the perspective view of the proposed electro-absorption Si_3N_4/VO_2 modulator. The modulator consists of a thin VO_2 layer deposited on a Si_3N_4 waveguide resides on SiO_2 substrate. A single layer graphene sheet is placed on the VO_2 layer as a heater to provide the required heat for a VO_2 phase transition. Two gold/titanium (Au/Ti) pads are used to obtain the low contact resistance between the Ti and graphene and they are considered to be far enough from waveguide core to prevent excess optical loss. The length of the VO_2 layer as well as and graphene is L. Fig. 1(b) shows the cross-section view of the hybrid Si_3N_4/VO_2 modulator with the thickness of VO_2 labeled as t. The design of the modulator starts with a Si_3N_4 waveguide with a cross-section of $w \times h = 600 \times 250$ nm^2.

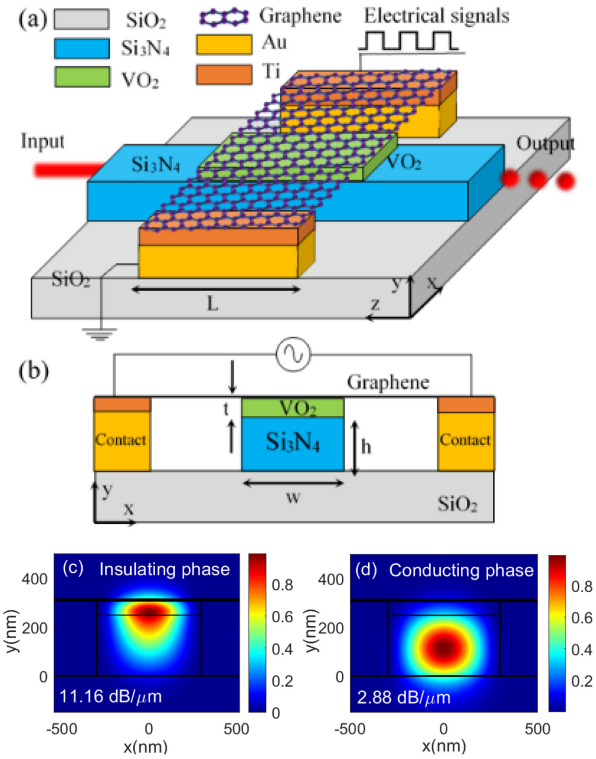

Fig. 1. (a) Perspective view and (b) cross-sectional view of the proposed hybrid Si_3N_4/VO_2 modulator. The optical mode of Si_3N_4/VO_2 hybrid waveguide when VO_2 is in the (c) insulting and (d) conducting phase.

These dimensions are chosen to ensure that the waveguide supports only one transverse-electric (TE) mode at a wavelength of 850 nm. The refractive index of SiO_2, and Si_3N_4 are 1.45 [39], 2.02 [40], respectively, at $\lambda = 850$ nm. Also, the wavelength dispersion of the refractive indices has been taken into account in our simulations. The device simulation is conducted using a three-dimensional finite-difference time-domain (3D FDTD) method.

The operation of the proposed modulator can be described as follows. When no current is injected, the VO_2 is in an insulating phase with the refractive index of $2.90 + 0.46i$ (at $\lambda = 850$ nm) [14]. Since the real part of the refractive index of VO_2 (in its insulating phase) is larger than that of Si_3N_4, the optical mode of the waveguide is mainly confined in the VO_2 layer as clearly shown in Fig. 1(c). Because of the relatively large imaginary part of VO_2 and the field confinement in this layer, the designed waveguide will have large propagation loss when the VO_2 is in the insulating phase and attenuates the propagating optical wave. We denote this case as the OFF-state of the proposed modulator. On the other hand, when sufficient voltage is applied to the electrical contacts of Fig. 1(a), the injection of electrical current through the graphene micro-heater will increase the temperature of this layer and its undelying VO_2 region. Once the temperature of the VO_2 layer rises above the threshold value $T_{\rm th} = 68^\circ$ C, it initiates the insulating to the conducting phase transition.

When VO_2 is in the conducting phase, as can be seen from Fig. 1(d), the light will be mainly confined in the Si_3N_4 region because of its higher refractive index compared to the VO_2

(which is $1.82 + 0.87i$ [14]). However, the waveguide mode will have a finite propagation loss because of the field penetration in the metallic VO_2 layer. In what follows we call this situation the ON-state of the active waveguide. Also, it may be noted that the presence of the ultra-thin graphene microheater (with the thickness of 0.34 nm) does not affect the optical modes of the active waveguide and therefore does not cause any excess propagation loss. In the next section, we will first find the optimum thickness of the VO_2 layer that results in the maximum extinction ratio for an active waveguide with a unit length of 1 μm. Then the optical performance of the designed modulator (in terms of optical bandwidth, insertion loss and extinction ratio) will be examined through simulations. Finally, the VO_2 heating process will be simulated and required actuating electrical power and VO_2 phase transition time will be calculated.

III. Optical and Electrical Properties of the Modulator

To find the optimum thickness of the VO_2 layer we sweep this parameter in the range of 10 nm $< t <$ 350 nm, and calculate the optical loss of a 1 μmlong active waveguide (when the VO_2 is in conducting and insulating phase). In these calculations the input and output waveguides are Si_3N_4 strip waveguides with the dimensions of 600×250 nm^2 and the coupling loss between the Si_3N_4 strip and the active waveguide is taken into account. The results are presented in Fig. 2(a) showing that when VO_2 is in the insulating phase (waveguide OFF-state) for $t < 60$ nm the insertion loss rapidly increases by increasing the thickness of the VO_2, then it decreases for 60 nm $< t <$ 150 nm and eventually reaches the value of 6 dB/μm for larger VO_2 thicknesses. For the ON-state, the insertion loss increases for $t < 100$ nm and then approaches the value of $\sim$3 dB/μm for larger t values.

The behavior of the waveguide propagation loss in the OFF-state can be attributed to the excitation of the higher-order modes. For $t < 60$ nm, the hybrid Si_3N_4/VO_2 waveguide only supports the fundamental TE mode (TE_{00}). As can be seen in Fig. 2(b) a significant portion of the field profile of this mode is localized in the VO_2 layer (because of the refractive index contrast between Si_3N_4 and VO_2). Therefore, an increase in the VO_2 thickness which is an absorptive media leads to higher propagation loss values. For $t > 60$ nm, on the other hand, the active waveguide also supports higher-order modes. For example, as depicted in Fig. 2(b), for $t = 150$ nm waveguide supports three TE modes (TE_{00}, TE_{10}, and TE_{01}), and for $t = 300$ nm waveguide supports four TE modes (TE_{00}, TE_{10}, TE_{01}, and TE_{02}). This means that for $t > 60$ nm, the input power will be divided between multiple modes of the active waveguide that have different propagation losses (propagation loss of different modes at $\lambda = 850$ nm is also provided in Fig. 2(b)). The propagation loss of each mode and the power coupled to each mode varies by the thickness of the VO_2 layer and as a result the overall insertion loss of the waveguide changes as depicted in Fig. 2(a).

The extinction ratio (ER) of the active waveguide section defined as the difference between insertion losses of the OFF-state and ON-state; $ER = IL_{OFF} - IL_{ON}$, is also plotted in Fig. 2(a) for different values of the VO_2 thickness. According to this figure, the largest reachable extinction ratio for the proposed structure is ER = 8.28 dB/μm and it can be achieved with the VO_2 thickness of $t = 60$ nm. This extinction ratio is comparable to the largest values reported for PCM based optical modulators [22]. The corresponding insertion loss of the structure which is the insertion loss of the ON-state is also IL = 2.88 dB/μm. The field profile of the propagating wave in the proposed waveguide (with $t = 60$ nm), when VO_2 is in the insulating and conducting phase us presented in Fig. 3(a) and (b), respectively. As can be seen, when the waveguide is in OFF-state (VO_2 is in insulating phase) it highly attenuates the propagating wave and when it is in ON-state induces a finite insertion loss.

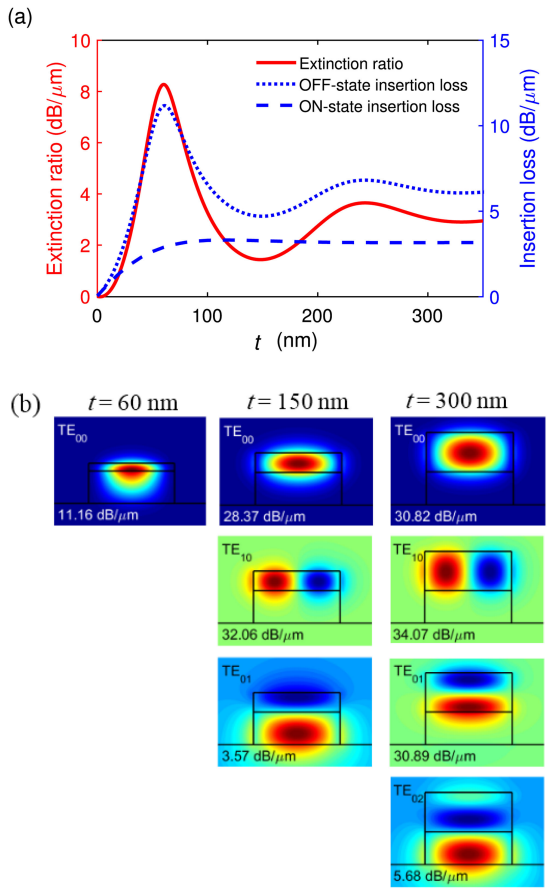

Fig. 2. The extinction ratio and insertion loss of the proposed modulator in the OFF- and ON-state, as a function of the VO_2 width; w. (b) the electric field profiles of the supported mode of hybrid Si_3N_4/VO_2 waveguide for different VO_2 thicknesses t.

Fig. 4 shows the insertion loss spectrum of the modulator (a 1-μm active waveguide inserted in a Si_3N_4 strip waveguide) in the ON- and OFF-states in the wavelength range of 800–900 nm. The difference between the insertion losses of these two states is also presented as the ER. The insertion losses are slowly varying functions of the wavelength and therefore the ER slightly changes for 800 nm $< \lambda <$ 900 nm. The extinction ratio reaches its maximum value of $\sim$8.35 dB/μm at $\lambda = 870$ nm and remains above 7.7 dB/μm in the specified wavelength range.

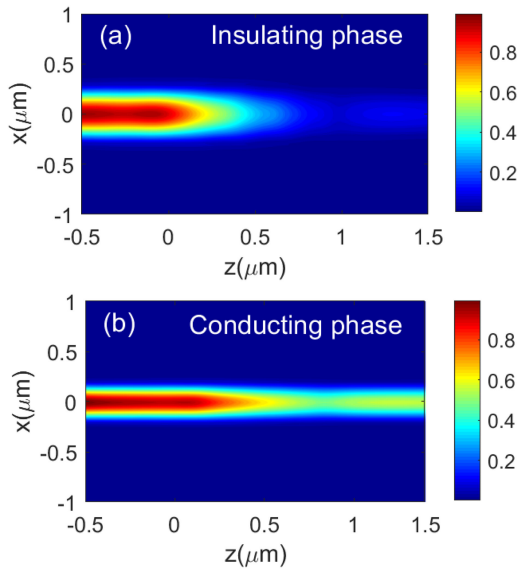

Fig. 3. Top views of light propagation through the Si_3N_4/VO_2 hybrid modulator with VO_2 in different phases at 850 nm: (a) insulating phase and (b) conducting phase, where $t = 60$ nm, and $L = 1$ μm.

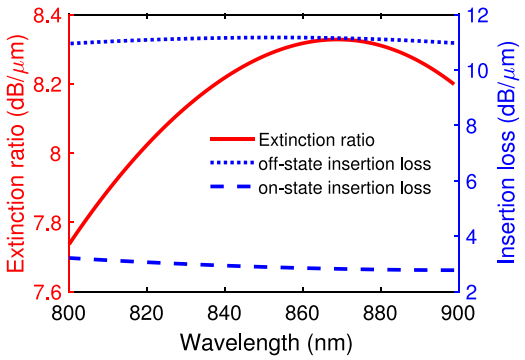

Fig. 4. The extinction ratio, OFF-state and ON-state insertion loss of the proposed modulator for the wavelength range of 800 nm to 900 nm, where $t = 60$ nm.

To highlight the advantages of using the graphene microheater instead of a metallic heater we also simulate the same active waveguide (with VO_2 thickness of 60 nm) when a 100 nm layer of Ti or Au is used as the heater element. In these cases, the metallic layer pushes the electric field away from its underlying layer (the VO_2 layer) and hence reduces the field confinement in the VO_2. As a result, the difference between the insertion losses of the active waveguide in its ON- and OFF-states decreases and the extinction ratio is below ~3 dB and 2 dB for Ti and Au heaters, respectively. The ER for the case of Ti and Au heaters can be increased to ~5 dB and 6 dB by redesigning the waveguide and increasing the VO_2 thickness to $t = 100$ nm that are again lower than ER of the structure with a graphene microheater. Also, a thicker VO_2 layer requires higher thermal power for phase transition and its transition takes more time.

The heating power generated by applying an electrical current/voltage to the contacts of structure in Fig. 1 is related to the total resistance between the two metal contacts; R_t and the injected current I as; $P_h = I^2 R_t$. The total resistance R_t is the sum of the resistance of the graphene layer R_G and the contact resistance between the graphene layer and the metal pads R_c, and can be calculated as; $R_t = R_G + 2R_c = (R_s d + 2R_c)/L$. The reported values for the sheet resistance of graphene, R_s and the Ti/graphene contact resistance are; $R_s = 1.7$ k$\Omega/\square$, and $R_c = 800\,\Omega \cdot \mu$m [30]. The total resistance of the proposed 1 μmlong device then is $R_t = (4.42\,\text{k}\Omega + 2 \times 0.8\,\text{k}\Omega) = 5\,\text{k}\Omega$. The portion of the heating power dissipated in graphene and Ti contacts is $P_G = P_h \times R_G/(R_G + 2R_c)$ and $P_c = P_h \times 2R_c/(R_G + 2R_c)$, respectively. Therefore, as it can be seen the main part of the heating power is dissipated in the graphene layer and will be transferred to the underlying VO_2 region. It may be noted that lower contact resistances have been also reported, which means that the unwanted power consumption in the contacts can be further reduced [41].

To simulate the insulating to the conducting phase transition of the VO_2 (corresponding to the modulator OFF-state to ON-state transition) we apply an electrical voltage pulse with the duration of 100 ns and power of 1.5 mW to the contact of the structure and calculate the temperature distribution. Fig. 4 shows the transient heating process, where the temperature is measured at the interface of Si_3N_4 and VO_2 that is at the furthest distance from the graphene heater and its temperature is lower than the rest of the VO_2 layer. In these simulations, the heat transfer equation and electric current flow equation are solved together using the finite element method. The thermal conductivity and heat capacity of monolayer graphene (with the thickness of 0.34 nm) is set to 4000 $\text{Wm}^{-1}\text{K}^{-1}$ and 2082 $\text{J·kg}^{-1}\text{K}^{-1}$, respectively [36], and the thermal parameters of the VO_2 and SiO_2 and Si_3N_4 are respectively from [42] and [7]. It can be seen that the temperature of the VO_2 increases from the room temperature ($T = 300$°K) to its threshold value of 68°C in less than 100 ns and when the input electrical pulse returns to zero (at $t = 100$ ns) the VO_2 temperature reduces to the room temperature in less than 200 ns.

Calculated values for the VO_2 heating and cooling time (100 ns and 200 ns, respectively), and also the required actuation power is lower than the previously reported values for the structures incorporating a Joule heating mechanism for the VO_2 phase transition [22]. This can be attributed to the fact that here the temperature of the heating layer (mono-layer graphene sheet) increases very fast and the produced heat is directly transferred to the VO_2 layer. The temperature of the graphene layer and the temperature at the center of the Si_3N_4 ridge is also plotted in the inset of Fig. 4. According to this figure, during the heating process, the temperature of the graphene microheater and the Si_3N_4 surface reach the maximum values of 77 °C and 64 °C, respectively. It should be mentioned that this temperature rise does not change the refractive index of Si_3N_4 because of its low thermo-optic coefficient of $dn/dT = 2.5 \times 10^{-5}$ K^{-1} [6]. Similarly, the conductivity of the graphene varies slightly in the temperature range of interest [43] so that the results remain approximately unchanged.

The spatial temperature distribution in the graphene, VO_2 and the Si_3N_4 layer is presented in Fig. 5. In this figure, the temperature is presented at the end of the input actuation pulse (i.e. $t = 100$ nm) when the temperature of each layer reaches its maximum value. Two cut lines of 1 and 2 are marked in Fig. 5(a) and the cross-sectional view of the temperature distribution along these cut lines are presented in Fig. 5(b) and (c),

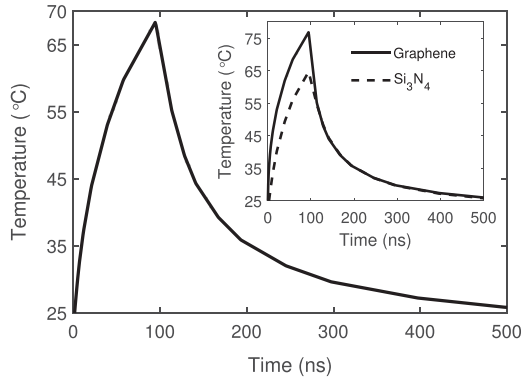

Fig. 5. The temperature in the VO_2/Si_3N_4 interface as a function of time for an actuation electrical pulse with the power of 1.5 mW and a duration of 100 ns. The inset shows the temperature variation of the graphene and at the center Si_3N_4 layer.

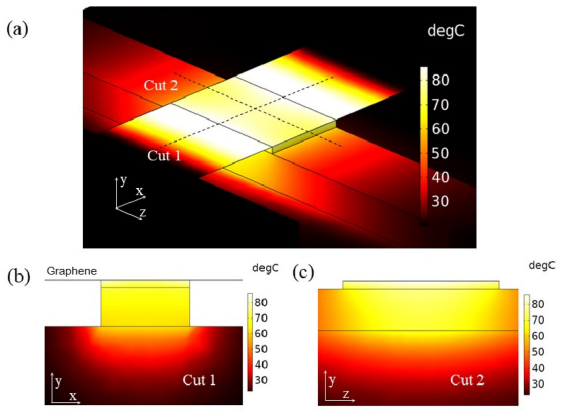

Fig. 6. (a) Three-dimension spatial temperature distribution in the proposed modulator structure. (b) and (c) Temperature distribution for the cross-sections along Cut 1 and Cut 2 [in Fig. (a)], respectively, 100 ns after applying the actuating electrical pulse.

respectively. As can be seen, the temperature of the whole VO_2 layer is raised above 68 °C which ensures the heat-induced phase transition. Note that the temperature in the graphene region that is in contact with VO_2 is lower than the temperature of the suspended graphene region which shows the fast heat transfer from graphene to the VO_2 layer.

IV. Conclusion

We have proposed a compact wideband hybrid Si_3N_4/VO_2 electro-absorption modulator for operation at the communication wavelength of 850 nm. In the proposed structure the optical amplitude modulation was achieved through the thermally triggered phase transition of the VO_2 layer. To decrease the triggering time and the required actuation energy, a mono-layer graphene microheater was designed. 3D-FDTD simulation of the designed modulator showed the ER of ∼8.3 dB/μm and the IL of ∼2.8 dB/μm at $\lambda = 850$ nm. Furthermore, the ER of the modulator remains above 7.7 dB/μm in the wide wavelength range of 800900 nm. Electro-thermal simulation of the structure also revealed that fast transition times of 100 ns and 200 ns for insulating-to-conducting and reverse phase transition of the VO_2, respectively, can be achieved by applying an electrical pulse with the power of 1.5 mW to the structure. Mentioned transition speeds show improvement over previously reported values for VO_2based modulators with Joule heating actuation. The results of this manuscript show the potential of the proposed modulator for use in configurable photonics integrated circuits.

References

[1] A. Rahim *et al.*, "Expanding the silicon photonics portfolio with silicon nitride photonic integrated circuits," *J. Lightw. Technol.*, vol. 35, no. 4, pp. 639–649, Feb. 2017.
[2] A. Z. Subramanian *et al.*, "Near-infrared grating couplers for silicon nitride photonic wires," *IEEE Photon. Technol. Lett.*, vol. 24, no. 19, pp. 1700–1703, Oct. 2012.
[3] S. Romero-García, F. Merget, F. Zhong, H. Finkelstein, and J. Witzens, "Silicon nitride CMOS-compatible platform for integrated photonics applications at visible wavelengths," *Opt. Express*, vol. 21, no. 12, pp. 14036–14046, Jun. 2013.
[4] D. Martens *et al.*, "Compact silicon nitride arrayed waveguide gratings for very near-infrared wavelengths," *IEEE Photon. Technol. Lett.*, vol. 27, no. 2, pp. 137–140, Jan. 2015.
[5] G. Gao *et al.*, "Silicon nitride O-band (de)multiplexers with low thermal sensitivity," *Opt. Express*, vol. 25, no. 11, pp. 12260–12267, May 2017.
[6] J. Joo, J. Park, and G. Kim, "Cost-effective 2 × 2 silicon nitride Mach-Zehnder interferometric (MZI) thermo-optic switch," *IEEE Photon. Technol. Lett.*, vol. 30, no. 8, pp. 740–743, Apr. 2018.
[7] P. Muñoz *et al.*, "Silicon nitride photonic integration platforms for visible, near-infrared and mid-infrared applications," *Sensors*, vol. 17, no. 9, pp. 1–25, Sep. 2017.
[8] C. T. PhareY.-H. Daniel Lee,, J. Cardenas, and M. Lipson, "Graphene electro-optic modulator with 30 GHz bandwidth," *Nat. Photon.*, vol. 9, p. 511, 2015.
[9] L. A. Shiramin and D. V. Thourhout, "Graphene modulators and switches integrated on silicon and silicon nitride waveguide," *IEEE J. Sel. Top. Quantum Electron.*, vol. 23, no. 1, pp. 94–100, Jan./Feb. 2017.
[10] A. Hermans *et al.*, "Integrated silicon nitride electro-optic modulators with atomic layer deposited overlays," *Opt. Lett.*, vol. 44, no. 5, pp. 1112–1115, Mar. 2019.
[11] W. Jin, R. G. Polcawich, P. A. Morton, and J. E. Bowers, "Piezoelectrically tuned silicon nitride ring resonator," *Opt. Express*, vol. 26, no. 3, pp. 3174–3187, May 2018.
[12] K. Alexander *et al.*, "Nanophotonic Pockels modulators on a silicon nitride platform," *Nat. Commun.*, vol. 9, no. 1, pp. 05846–05851, 2018.
[13] Y. H. D. Lee and M. Lipson, "Back-end deposited silicon photonics for monolithic integration on CMOS," *IEEE J. Sel. Top. Quantum Electron.*, vol. 19, no. 2, pp. 409–416, Mar./Apr. 2013.
[14] H. W. Verleur, A. S. Barker, and C. N. Berglund, "Optical properties of VO_2 between 0.25 and 5 eV," *Phys. Rev.*, vol. 172, no. 3, pp. 788–798, 1968.
[15] B. Janjan, M. Miri, A. Zarifkar, and M. Heidari, "Design and simulation of compact optical modulators and switches based on $SiVO_2$ Si horizontal slot waveguides," *J. Lightw. Technol.*, vol. 35, no. 14, pp. 3020–3028, 2017.
[16] I. Olivares *et al.*, "Optical switching in hybrid VO_2/Si waveguides thermally triggered by lateral microheaters," *Opt. Express*, vol. 26, no. 10, pp. 12387–12395, May 2018.
[17] K. J. Miller, K. A. Hallman, R. F. Haglund, and S. M. Weiss, "Silicon waveguide optical switch with embedded phase change material," *Opt. Express*, vol. 25, no. 22, pp. 26527–26536, Oct. 2017.
[18] R. M. Briggs, I. M. Pryce, and H. A. Atwater, "Compact silicon photonic waveguide modulator based on the vanadium dioxide metal-insulator phase transition," *Opt. Express*, vol. 18, no. 11, pp. 11192–11201, May 2010.
[19] K. Shibuya *et al.*, "Silicon waveguide optical modulator driven by metal–insulator transition of vanadium dioxide cladding layer," *Opt. Express*, vol. 27, no. 4, pp. 4147–4156, 2019.
[20] A. Joushaghani *et al.*, "Sub-volt broadband hybrid plasmonic-vanadium dioxide switches," *Appl. Phys. Lett.*, vol. 102, no. 6, p. 61101, Feb. 2013.
[21] B. A. Kruger, A. Joushaghani, and J. K. S. Poon, "Design of electrically driven hybrid vanadium dioxide (VO_2) plasmonic switches," *Opt. Express*, vol. 20, no. 21, pp. 23598–23609, Oct. 2012.
[22] K. J. Miller, R. F. Haglund, and S. M. Weiss, "Optical phase change materials in integrated silicon photonic devices: Review," *Opt. Mater. Express*, vol. 8, no. 8, pp. 2415–2429, Aug. 2018.

[23] M. Singh and A. Datta, "Modeling of a vertical hybrid plasmonic switch with VO_2 fin Bragg grating," *IEEE Photon. Technol. Lett.*, vol. 30, no. 11, pp. 997–1000, Jun. 2018.

[24] B. Wu *et al.*, "Electric-field-driven phase transition in vanadium dioxide," *Phys. Rev. B*, vol. 84, no. 24, pp. 241410–241413, Dec. 2011.

[25] P. Markov *et al.*, "Optically monitored electrical switching in VO_2," *ACS Photon.*, vol. 2, no. 8, pp. 1175–1182, Jul. 2015.

[26] S. Mohammadi-Pouyan, M. Miri, and M. H. Sheikhi, "Design of a vanadium dioxide-based dual-polarization optical PAM4 modulator," *J. Opt. Soc. Am. B*, vol. 35, no. 12, pp. 3094–3103, Dec. 2018.

[27] M. Sadeghi, B. Janjan, M. Heidari, and D. Abbott, "Mid-infrared hybrid Si/Vo_2 modulator electrically driven by graphene electrodes," *Opt. Express*, vol. 28, pp. 9198–9207, Mar. 2020.

[28] A. Zylbersztejn and N. F. Mott, "Metal-insulator transition in vanadium dioxide," *Phys. Rev. B*, vol. 11, no. 11, pp. 4383–4395, Jun. 1975.

[29] A. Shadmani, M. Miri, and S. Mohammadi Pouyan, "Ultra-wideband multi-level optical modulation in a $Ge_2Sb_2Te_5$-based waveguide with low power consumption and small footprint," *Opt. Commun.*, vol. 439, pp. 53–60, May 2019.

[30] P. Avouris and M. Freitag, "Graphene photonics, plasmonics, and optoelectronics," *IEEE J. Sel. Top. Quantum Electron.*, vol. 20, no. 1, pp. 72–83, Jan.–Feb. 2014.

[31] S. J. Koester and M. Li, "Waveguide-coupled graphene optoelectronics," *IEEE J. Sel. Top. Quantum Electron.*, vol. 20, no. 1, pp. 84–94, Jan.–Feb. 2014.

[32] M. Heidari and V. Ahmadi, "Design and analysis of a graphene magneto-plasmon waveguide for plasmonic mode switch," *IEEE Access*, vol. 7, pp. 43406–43413, 2019.

[33] B.-H. Huang, W.-B. Lu, X.-B. Li, J. Wang, and Z. guo Liu, "Waveguide-coupled hybrid plasmonic modulator based on graphene," *Appl. Opt.*, vol. 55, no. 21, pp. 5598–5602, Jul. 2016.

[34] A. A. Balandin *et al.*, "Superior thermal conductivity of single-layer graphene," *Nano Lett.*, vol. 8, no. 3, pp. 902–907, Apr. 2008.

[35] S. Yan *et al.*, "Slow-light-enhanced energy efficiency for the graphene microheater on silicon photonic crystal waveguides," *Nat. Commun.*, vol. 8, pp. 14411–14418, Feb. 2017.

[36] S. Gan *et al.*, "A highly efficient thermo-optic microring modulator assisted by graphene," *Nanoscale*, vol. 7, no. 47, pp. 20249–20255, Nov. 2015.

[37] L. Yu, Y. Yin, Y. Shi, D. Dai, and S. He, "Thermally tunable silicon photonic microdisk resonator with transparent graphene nanoheaters," *Optica*, vol. 3, no. 2, pp. 159–166, Feb. 2016.

[38] H. Kaushal and G. Kaddoum, "Optical communication in space: Challenges and mitigation techniques," *IEEE Commun. Surveys Tut.*, vol. 19, no. 1, pp. 57–96, 2017.

[39] E. Palik, *Handbook of Optical Constants of Solids: Volume 1*. Elsevier Science, 2012.

[40] K. Luke, Y. Okawachi, M. R. E. Lamont, A. L. Gaeta, and M. Lipson, "Broadband mid-infrared frequency comb generation in a Si_3N_4 microresonator," *Opt. Lett.*, vol. 40, no. 21, pp. 4823–4826, May 2015.

[41] F. Giubileo and A. Di Bartolomeo, "The role of contact resistance in graphene field-effect devices," *Prog. Surf. Sci.*, vol. 92, no. 3, pp. 143–175, Jun. 2017.

[42] G. V. Chandrashekhar, H. L. C. Barros, and J. M. Honig, "Heat capacity of VO_2 single crystals," *Materials Res. Bull.*, vol. 8, no. 4, pp. 369–374, 1973.

[43] Y. Francescato, V. Giannini, and S. A. Maier, "Strongly confined gap plasmon modes in graphene sandwiches and graphene-on-silicon," *New J. Phys.*, vol. 56, no. 15, pp. 1717–1723, 2013.

Babak Janjan was born in Nahavand, Iran, on February 1989. He received the B.Sc. degree from Isfahan University, Isfahan, Iran, in 2012, and the M.Sc degree from Shiraz University, Shiraz, Iran, in 2015 both in electrical engineering. He is currently pursuing the Ph.D. degree in electrical engineering with Tarbiat Modares University, Tehran, Iran. His current research interests include integrated optics and nonlinear optics.

Mehdi Miri was born in Shiraz, Iran, on October 26, 1983. He received the B.Sc. degree in electrical engineering from Shiraz University, Shiraz, Iran in 2006, and the M.Sc., and Ph.D. degrees from the Sharif University of Technology, Tehran, Iran, in 2008, and 2013, respectively, both in electrical engineering. Since then, he has been with the School of Electrical and Computer Engineering, Shiraz University, as an Associate Professor. His research interests include integrated optics and nanoelectronics.

Davood Fathi received the B.Sc. degree in the field of electronic engineering from the Amirkabir University of Technology, Tehran, Iran, in 1990, and the M.Sc. degree in the field of biomedical engineering from the Sharif University of Technology, Tehran, in 1994. After a couple of years working in industry, he worked toward the Ph.D. degree between 2006-2009 in the field of nanoelectronics with the Nanoelectronic Center of Excellence, Thin Film and Photonics Research Laboratory, School of Electrical and Computer Engineering, University of Tehran, Tehran. Dr. Fathi has joined from 2010 as a member of faculty to the Department of Electrical and Computer Engineering, Tarbiat Modares University (TMU), Tehran. His current research interests include: nanoelectronics; nanophotonics and optoelectronics; nanobiophotonics; computational optics-photonics; and solar cells. He is also author or coauthor of more than 75 journal and conference papers in various fields of nanoelectronics and nanophotonics. Dr. Fathi is currently an Associate Professor of photonics and optoelectronics at his department.

Mohsen Heidari was born in Shiraz, Iran, on August 1989. He received the B.S. and M.S. degrees in electrical engineering from the Department of Communication and Electronic Engineering, Shiraz University, Shiraz, Iran, in 2011 and 2013, and Ph.D. degree in electrical engineering from Tarbiat Modares University (TMU), Tehran, Iran, in 2019. His current research interests include graphene and 2D materials-based plasmonic and magneto-plasmonic, all-optical switches and modulators, plasmonic isolators, and nano-photonic devices.

Derek Abbott (Fellow, IEEE) was born in South Kensington, London, U.K., in 1960. He received the B.Sc. (Hons.) degree in physics from Loughborough University, U.K., in 1982, and the Ph.D. degree in electrical and electronic engineering from the University of Adelaide, Australia, in 1997, under the supervision of K. Eshraghian and B. R. Davis. His research interests include the areas of multidisciplinary physics and electronic engineering applied to complex systems. His research programs span a number of areas of stochastics, game theory, photonics, energy policy, biomedical engineering, and computational neuroscience. He is a fellow of the Institute of Physics, U.K., and an Honorary Fellow of Engineers Australia.

He received a number of awards, including the South Australian Tall Poppy Award for Science, in 2004, an Australian Research Council Future Fellowship, in 2012, the David Dewhurst Medal, in 2015 the Barry Inglis Medal, in 2018, and the M. A. Sargent Medal for eminence in engineering, in 2019. He has served as an Editor and/or a Guest Editor for a number of journals, including the IEEE JOURNAL OF SOLID-STATE CIRCUITS, *Journal of Optics B*, *Chaos*, *Fluctuation and Noise Letters*, PROCEEDINGS OF THE IEEE, and the IEEE PHOTONICS JOURNAL. He has served on the board of PROCEEDINGS OF THE IEEE, and is currently on the Editorial Boards of *Scientific Reports* (Nature), *Royal Society OS*, *Frontiers in Physics* and IEEE ACCESS. He serves on the IEEE Publication Services and Products Board (PSPB) and is the current Editor-in-Chief (EIC) of IEEE ACCESS.